INTERFEROMETRIC PROCESSING OF A DEVELOPED MIMO GBSAR FOR DISPLACEMENT MONITORING

B. Hosseiny [1], J. Amini [1, *], H. Aghababaei [2]

[1] School of Surveying and Geospatial Engineering, Faculty of Engineering, University of Tehran, Tehran, Iran - (ben.hosseiny, jamini)@ut.ac.ir
[2] Department of Earth Observation Science (EOS), Faculty of Geo-Information Science and Earth Observation (ITC), University of Twente, 7514 AE Enschede, The Netherlands - h.aghababaei@utwente.nl

Commission IV, WG IV/3

KEY WORDS: structural monitoring, terrestrial radar interferometry, synthetic aperture radar (SAR), W band radar, mmWave, deformation, ground-based radar

ABSTRACT:

This study demonstrates the interferometric processing experiments of our developed multiple-input multiple-output ground-based synthetic aperture radar (MIMO GBSAR) system. GBSAR systems are known as precise noncontact instruments for monitoring earth dynamics. In recent years W band MIMO radars have shown interesting potential in this field due to their low cost, compact size, and high phase sensitivity. MIMO capability enables the angular discrimination of multiple targets in the same range as the radar sensor. In our previous works, we developed a high-resolution MIMO GBSAR system based on the combination of MIMO radar and mechanical rail. Accordingly, this study investigates the developed system's displacement monitoring capability by presenting a controlled experiment, using fixed and moving corner reflectors and gathering 36 time series of data. We compare and discuss the results obtained from MIMO GBSAR and MIMO radar configurations. The results show that our developed system highly agrees with MIMO radar's interferometric measurements while providing a better target discrimination capability and higher signal noise ratio.

1. INTRODUCTION

Radar remote sensing has been widely employed in monitoring and earth observation applications because it is least sensitive to weather conditions. Radar data is divided into amplitude and phase, with the amplitude containing physical qualities and the phase relating to the monitoring scene's range information. Due to the radar's phase's sensitivity to target range, techniques for deriving target movement or height information through the interference of at least two signal phase measurements have been proposed. Accordingly, Surface and structural displacement monitoring is the primary purpose of radar interferometry. Moreover, synthetic aperture radar (SAR) imaging capability has enabled high-resolution radar imaging by coherently integrating received signals to the receiver antenna at different along-track locations (Carrara et al., 1995).

Radar sensors are mainly mounted on spaceborne, airborne, or ground-based platforms. Ground-based synthetic aperture radar (GBSAR) implementation and development have had a significant impact on remote sensing applications over the last two decades. This system incorporates a radar sensor that transmits and receives electromagnetic waves and repeats this operation as mainly it moves along a mechanical rail (Monserrat et al., 2014). The key factor in improving cross-range resolution is rail length, where increasing rail length leads in a narrower synthetic beamwidth and hence higher resolution (Carrara et al., 1995).

Increasing the applicability of GBSARs for remote sensing applications have led to the development of new systems and processing tools (Pieraccini and Miccinesi, 2019). Multiple-input multiple-output (MIMO) array geometry increases the radar's cross-range resolution with fewer antennas than phased array traditional geometry. Indeed, MIMO is made up of N_{RX} receiver antennas with Nyquist spacing and N_{TX} transmitter antennas with non-Nyquist spacing. As a result of this geometry $N_{Rx} \times N_{Tx}$ virtual antennas are produced. Thus, this condition increases the angular resolution by reducing the number of physical antennas (Tarchi et al., 2012).

Ground-based systems can be used as supplement tools for environmental or structural monitoring applications, and they can overcome many of the major shortcomings of airborne and spaceborne systems. GBSAR has a high data collecting rate. A GBSAR can monitor a specific area of interest with a temporal resolution ranging from a few seconds to a few minutes. This capacity allows for the monitoring of fast-moving natural targets, enhancing time-series data coherency, and mitigating processing issues such as wrapped phases in interferometric processing (Monserrat et al., 2014). Furthermore, most GBSAR sensors use frequency-modulated continuous wave (FMCW) signals, which is advantageous for short-range applications and minimizes system size and cost (Charvat, 2014). Accordingly, GBSAR monitoring can be applied to various fields of earth observation problems. Linear SAR (LISA) was the first GBSAR that was used for cultural heritage (Rudolf et al., 1999) and dam displacement (Tarchi et al., 1999) monitoring. A comprehensive review of the other applications of GBSAR for earth observation, such as landslide and glacier monitoring, has been provided by (Wang et al., 2020).

For the sake of structural displacement monitoring, compared to the currently available contact and noncontact sensors, radar is

* Corresponding author

https://doi.org/10.5194/isprs-annals-X-4-W1-2022-301-2023

attractive due to its wide coverage and high sensitivity to displacement signals in contrast to its low sensitivity to weather conditions. However, currently used GBSAR systems for structural monitoring mainly operate in Ka or Ku frequencies with sub-millimeter sensitivity to displacements. Yet in most recent studies, W band MIMO radars, due to their low cost and compact size, have found ways in remote sensing applications, especially for structural monitoring (Miccinesi et al., 2021). These systems operate in the frequency range of 76-81 GHz and are mainly developed for automotive applications. However, their capabilities make them attractive for use in other fields of applications (Yanik et al., 2020). Recent studies by (Baumann-Ouyang et al., 2021) and (Ciattaglia et al., 2020) approve the applicability of these radars for structural monitoring with nearly micrometer accuracy. Moreover, few studies applied W band MIMO radars to monitor real-world objects such as bridges and other large structures (Pieraccini and Miccinesi, 2019; Rodrigues and Li, 2021).

The angular discriminability of MIMO radars is limited to the number of generated virtual arrays. Currently available W band MIMO radars provide low angular resolution while increasing the number of antennas cause more cost and complexity. In order to address this issue, one solution can be combining mechanical rail with a MIMO radar. In our previous studies we investigated the effectiveness of combining MIMO radar and mechanical rail on improving the target detection and interferometric measurements both with simulations (Hosseiny et al., 2021b) and real experiments (Hosseiny et al., 2021a). In this study our main objective is to evaluate and investigate the displacement measurement capabilities of our developed MIMO-GBSAR. In this system a W band MIMO radar is installed on a mechanical rail. The used radar sensor is AWR1642BOOST manufactured by Texas Instruments (TI). We show the results of various experiments and evaluate and discuss them from different aspects.

The rest of the paper is organized as follows: section 2 describes the utilized MIMO GBSAR system. Section 3 provides the required theoretical background of MIMO and SAR processing. In section 4, the results are presented and discussed. Finally, section 5 concludes and summarizes this study.

2. SYSTEM CONFIGURATION

Figure 1 shows the components of our developed MIMO GBSAR system. It consists of a radar sensor, data acquisition board, a two-axis linear stepper, and a personal computer (PC). The radar instrument is AWR1642BOOST, manufactured by TI. It consists of 4 receivers and 2 transmitter antennas in MIMO geometry. The operating signal is FMCW in the frequency range of 76-81 GHz. The maximum dedicated signal bandwidth is 4 GHz, providing a centimeter-level resolution in range direction.

After performing bandpass filtering, and dechirping, the received waveform is digitized, and the DCA1000EVM module by TI sends the digitized captured data to the PC through Ethernet.

The radar sensor is attached on a two-axis linear rail. This leads to higher cross-range resolution after processing the acquired signals. The maximum scanning ranges in vertical and horizontal rails are 50 cm and 90 cm, respectively. An Arduino microcontroller chip controls them. Notably, the stepper motor continuously moves on the horizontal axis and then moves one step with a fixed offset in the vertical direction after completing a horizontal scan. The mentioned system parameters are summarized in Table 1.

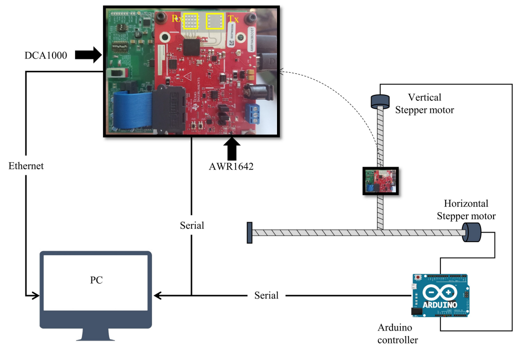

Figure 1. Schematic diagram of the developed MIMO GBSAR components

Parameter	Value
Radar model	TI-AWR1642BOOST
operating frequency (f_c)	76-81 GHz
Signal type	Linear FMCW
bandwidth (B)	4 GHz
Range samples	512
Sweep time (τ)	60 us
Number of receivers (N_{Rx})	4
Number of transmitters (N_{Tx})	2
Horizontal rail length (L_h)	0.9 m
Peak power (P)	1.5 mW
Vertical rail length (L_v)	0.5 m
Tx and Rx Gain (G)	30 dB

Table 1. MIMO GBSAR parameters

3. PRINCIPLES OF MIMO GBSAR

MIMO radar consists of N_{Rx} receiver antennas and N_{Tx} transmitter antennas. Compared to the uniform linear arrays, MIMO antennas provide a different geometry. The space between a pair of receiver antennas is half the wavelength, and the transmitter antennas are separated by N_{Rx} times the half wavelength. Consequently, appropriate MIMO beamforming on the received signals leads to N_{Rx}×N_{Tx} virtual transceicving antennas, which provides finer angular resolution than its phased array equivalent (Tarchi et al., 2012). The equivalent virtual array is located in the middle of its corresponding transmitter and receiver antennas (Guarnieri et al., 2022).

The received signals need to be orthogonal that means their inner product have to zero in order to be distinguished. This could be done through time-division or frequency-division (Baumann-Ouyang et al., 2021). We performed the first approach, which is also known as time division multiplexing (TDM). In this case all transmitter antennas transmit same frequency range, but at different times.

The received intermediate frequency signal of the i^{th} virtual antenna of MIMO radar is as follows (Gao et al., 2021):

$$s_{if}(i,t) = \exp\left\{ j2\pi\left(f_0\tau + k_r\tau t - \frac{k_r\tau^2}{2} + \frac{id\sin\theta}{\lambda} \right) \right\} \quad (1)$$

where $s_{if}(i,t)$ = received intermediate frequency signal
kr = chirp slope
f_0 = signal's starting frequency
λ = wavelength
τ = scattering target's time delay
θ = scattering target's cross-range angle
d = inter-distance of virtual arrays

According to the presented MIMO processing, TI AWR1642BOOST radar chip can synthesize 8 virtual arrays out of two transmitters and four receiver antennas MIMO beamforming. The resulting virtual arrays can provide roughly 15 degrees of angular resolution, which may be insufficient for high-resolution target discrimination. As we discussed in our previous study (Hosseiny et al., 2021c), MIMO beamforming enables us to increase the cross-range sampling interval with the factor of $N_{Tx}N_{Rx}$ without causing Aliasing. Thus, radar signal acquisition rate or sampling interval (Δx) should be smaller than the following equation:

$$\Delta x \leq \frac{N_{Tx}N_{Rx}\lambda}{4} \quad (2)$$

Raw MIMO GBSAR data matrix is generated After rearranging the received signal from the observing area. Afterward, a single look complex (SLC) image is generated by compressing signals in range and cross-range directions. Each pixel of the resulting image consists of amplitude and phase components, which represent the backscattered radar signal from the corresponding range and cross-range location. The phase component is sensitive to the respective target's range. Accordingly, line of sight (LOS) displacement can be retrieved by differentiating the phase of two SLC images, acquired at two different epochs:

$$\Delta R_{21} = R_2 - R_1 = \frac{\lambda\Delta\Phi_{21}}{4\pi} \quad (3)$$

where ΔR_{21} = LOS displacement
$\Delta\Phi_{21}$ = phase difference between pixels at time one and two
R_1,R_2 = target's range at time one and two

4. EXPERIMENTS AND RESULTS

Figure 2 shows the measurement setup and our developed GBSAR system. Two 10 cm trihedral corner reflectors were located in front of the radar, at a distance of about 7 m and 8 m, and with different cross-range locations. In this study, we only used a 10 cm synthetic aperture to avoid the defocusing effects of long synthetic aperture length in near-field targets due to the non-ideal imaging geometry. Our previous work has discussed the relation between the target range and the focusing performance of a SAR image (Hosseiny et al., 2022).

We operated a controlled scenario in order to demonstrate and evaluate the displacement measurement capability of the MIMO GBSAR system. In this experiment, one of the mentioned corner reflectors was fixed, and the other was displaced at about 0.5 mm in every 5 epochs during the measurements (see Figure 2).

A total of 36 repeat-pass signals were acquired from the observing scene. To derive the final displacement values from radar observations, the following processing steps were carried out for both MIMO radar and MIMO GBSAR configurations:
1- Generating SLC focused image from the raw collected by the range and cross-range compression of the signals at each epoch
2- Stacking the TS of SLC images
3- Detecting persistent scatterers from the pixels with amplitude dispersion index (ADI)<0.1 and amplitude of -10 dB from the maximum amplitude present in the image.
4- Generating PS mask
5- calculating the interferometric phase between two pairs of SLC images
6- Integrating the interferometric phases and calculating the final displacement based on Eq (3).

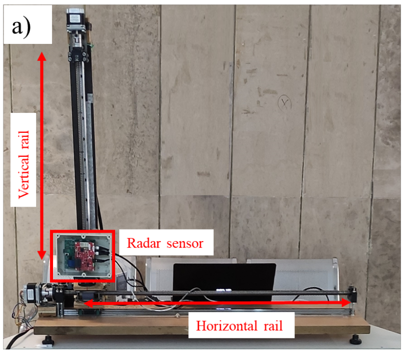

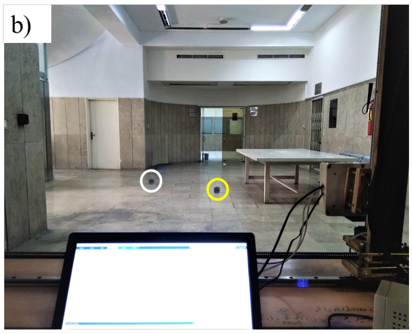

Figure 2. Measurement setup: (a) MIMO GBSAR system (b) Observing area. White and yellow circles denote fixed and moving corner reflectors, respectively.

Figure 3 shows the obtained results for MIMO radar configuration. Wide signal response of targets in cross-range direction is evident (see Figure 3-a). This is due to MIMO radar's small number of virtual arrays, which cannot afford cross-range resolution better than 15 degrees. Consequently, the ADI map, PS mask, and final displacement map obtained from the MIMO radar signals are shown in Figures 3-b, c, and d, respectively. Similarly, Figure 4 shows the results from the MIMO GBSAR configuration. We can notice that the targets' spread functions look much narrower than the MIMO radar's focused image (see Figure 4-a). Accordingly, the obtained results contain more details, and a higher number of targets are distinguishable in this configuration. Resulting in a better cross-range resolution of MIMO GBSAR, the obtained ADI map (Figure 4-b), PS mask (Figure 4-c), and final displacement map (Figure 4-d) provide more details than the MIMO radar results.

https://doi.org/10.5194/isprs-annals-X-4-W1-2022-301-2023 | © Author(s) 2023. CC BY 4.0 License.

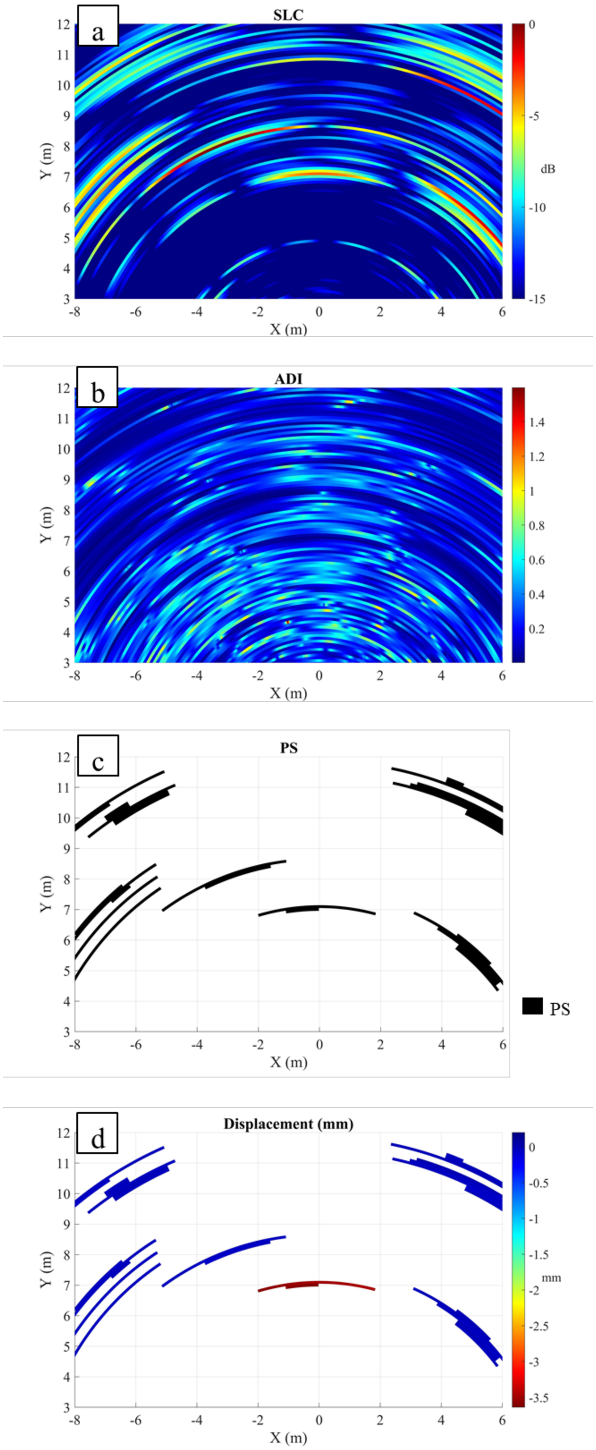

Figure 3. MIMO radar measurement results: (a) SLC image of the first epoch. (b) ADI of TS images (c) detected PS areas. (d) Displacement map

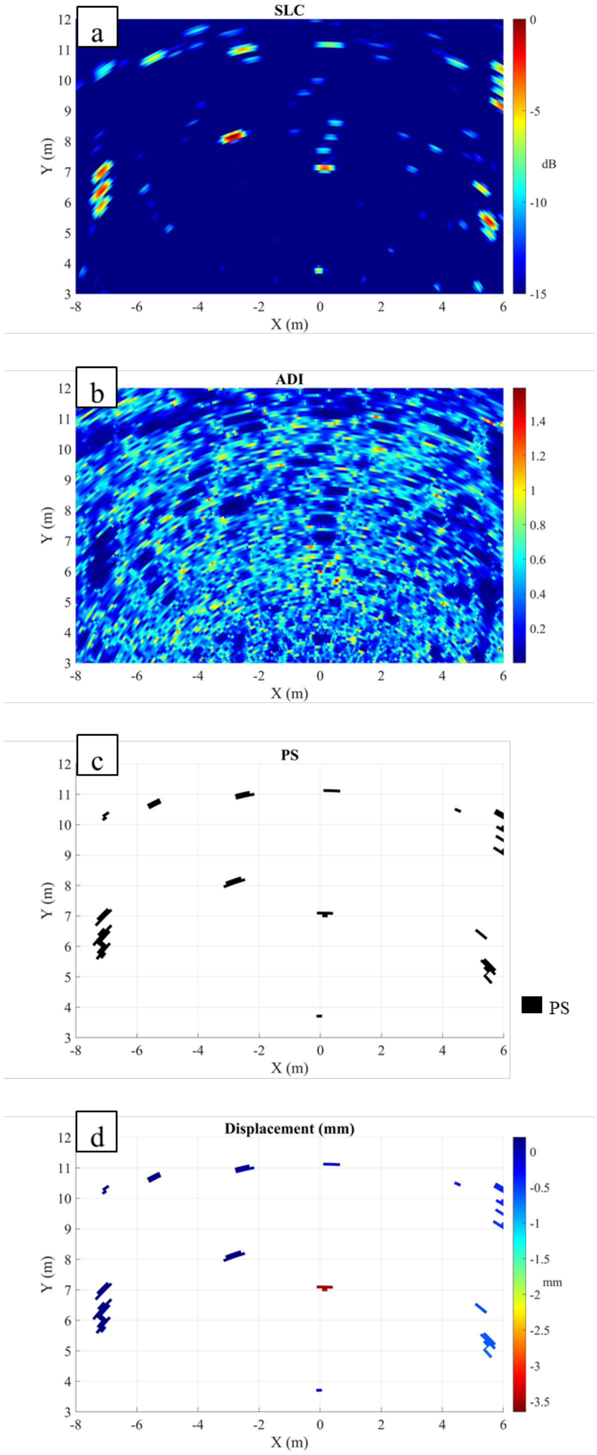

Figure 4. MIMO GBSAR measurement results: (a) SLC image of the first epoch. (b) ADI of TS images (c) detected PS areas. (d) Displacement map

Figure 5 shows the interferometric measurements of fixed and displaced corner reflectors during the time epochs from the processed signals of MIMO radar and MIMO GBSAR configurations. The displacement patterns obtained from MIMO GBSAR data for both fixed and displaced targets show a high correlation and agreement with the MIMO radar mode. More specifically, Figure 6 compares the interferometric measurements with reference values. As can be seen, MIMO radar measurements are closer to the reference values and, thus, are more accurate.

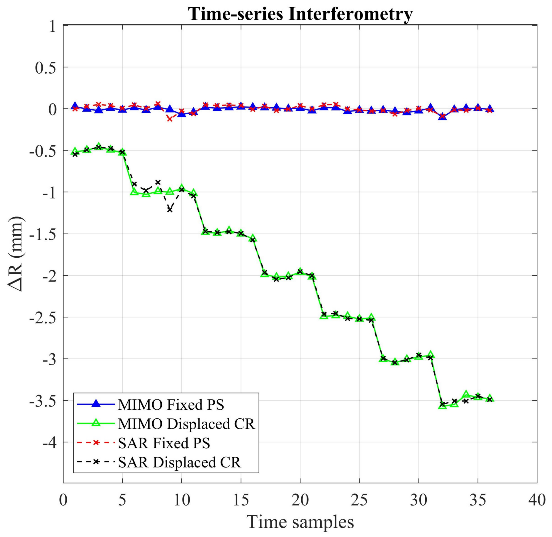

Figure 5. Time-series displacement measurements of deployed corner reflectors by MIMO radar and MIMO GBSAR signals.

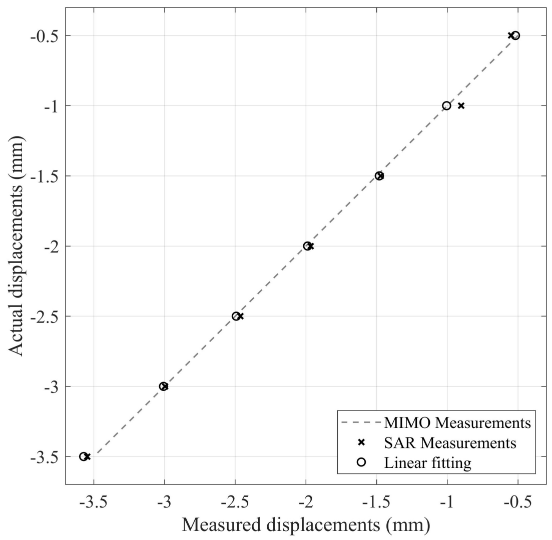

Figure 6. Comparison of MIMO radar and MIMO GBSAR displacement measurements with the reference values.

We also evaluated and compared the results of MIMO radar and MIMO GBSAR configurations, using several metrics in Table 2. MIMO GBSAR obtained 0.06 radian angular resolution, which is much higher than MIMO radar's 0.49 rad resolution. Moreover, the obtained peak sidelobe ratio (PSLR) and mean ADI approve the better performance of MIMO GBSAR in target focusing and signal-to-noise ratio.

MIMO radar obtained 0.0065 mm displacement standard deviation (std), demonstrating better stability than MIMO GBSAR (0.021 mm). Accordingly, based on Gaussian modelling (Baumann-Ouyang et al., 2021), the developed MIMO GBSAR can detect a minimum displacement signal of 0.126 mm with a 99.7% confidence level. However, the lower displacement accuracy of our developed MIMO GBSAR could be due to the mechanical rail's fluctuations and coregistration errors. We will evaluate them in more detail in our future work.

Metric	MIMO radar	MIMO GBSAR
Angular resolution (rad)	0.49	0.06
PSLR (dB)	4.4	5.7
Mean ADI	0.047	0.012
Displacement std (mm)	0.0065	0.021
MDD (mm)	0.039	0.126

Table 2. Quantitative comparison of MIMO radar and MIMO GBSAR TS interferometric measurements

5. CONCLUSION

W band MIMO radars have found increasing interest in recent studies of geo-sensors due to their low cost and compact size. Moreover, MIMO radars enable cross-range target discrimination, and the W band signal can provide centimeter resolution and high phase sensitivity due to its millimeter level wavelength. This study was focused on the interferometric processing and displacement monitoring capability of our developed MIMO GBSAR system. We increased the cross-range resolution of MIMO radar by mounting the sensor on a mechanical rail. We carried out a controlled experiment to validate our system using fixed and moving corner reflectors. According to the obtained results, our developed system provided better focusing and signal-to-noise ratio than MIMO radar, with PSLR of 5.7 dB and the mean ADI of 0.047 along the time series. The obtained interferometric measurements demonstrated a high agreement with MIMO radar measurements. The obtained displacement standard deviation from 36 measurements was 0.021 mm. Therefore, the overall results approve the interferometric monitoring capability of our developed MIMO GBSAR system. Future works will be dedicated to investigating the limitations and drawbacks of this system and improving the results.

REFERENCES

Baumann-Ouyang, A., Butt, J.A., Salido-Monzú, D., Wieser, A., 2021. MIMO-SAR Interferometric Measurements for Structural Monitoring: Accuracy and Limitations. Remote Sens. 2021, Vol. 13, Page 4290 13, 4290. doi.org/10.3390/RS13214290

Carrara, W.G., Goodman, R.S., Majewski, R.M., 1995. Spotlight synthetic aperture radar : signal processing algorithms. Artech House, Boston : Charvat, G.L., 2014. Small and short-range radar systems. CRC Press.

Ciattaglia, G., De Santis, A., Disha, D., Spinsante, S., Castellini, P., Gambi, E., 2020. Performance Evaluation of Vibrational Measurements through mmWave Automotive Radars. Remote Sens. 2021, Vol. 13, Page 98 13, 98. doi.org/10.3390/RS13010098

Gao, X., Roy, S., Xing, G., 2021. Mimo-sar: A hierarchical high-resolution imaging algorithm for mmwave fmcw radar in autonomous driving. IEEE Trans. Veh. Technol. 70, 7322–7334.

Guarnieri, A.M., Wang, J., Wang, Y., Li, Y., Huang, X., 2022. Fast Displacement Estimation of Multiple Close Targets with MIMO Radar and MUSICAPES Method. Remote Sens. 2022, Vol. 14, Page 2005 14, 2005. doi.org/10.3390/RS14092005

Hosseiny, B., Amini, J., Esmaeilzadeh, M., Nekoee, M., 2021a. Evaluating an S-band Ground-Based Synthetic Aperture Radar Imaging System for LFMCW SAR Processing. Earth Obs. Geomatics Eng. 5. doi.org/10.22059/EOGE.2021.306032.1084

Hosseiny, B., Amini, J., Safavi-Naeini, S., 2022. Comparison Study of Signal Processing Algorithms for 3D SAR Imaging of MM-WAVE GBSAR System. Eng. J. Geospatial Inf. Technol. 10, 69–87.

Hosseiny, B., Amini, J., Safavi-Naeini, S., 2021b. Evaluating the deformation monitoring capability of a ground based SAR system with MIMO antenna. Eng. J. Geospatial Inf. Technol. 9, 21–40.

Hosseiny, B., Amini, J., Safavi-Naeini, S., 2021c. Simulation and Evaluation of an mm-Wave MIMO Ground-Based SAR Imaging System for Displacement Monitoring, in: 2021 IEEE International Geoscience and Remote Sensing Symposium IGARSS. IEEE, pp. 8213–8216. doi.org/10.1109/IGARSS47720.2021.9553347

Miccinesi, L., Consumi, T., Beni, A., Pieraccini, M., 2021. W-band MIMO GB-SAR for Bridge Testing/Monitoring. Electronics 10, 2261.

Monserrat, O., Crosetto, M., Luzi, G., 2014. A review of ground-based SAR interferometry for deformation measurement. ISPRS J. Photogramm. Remote Sens. 93, 40–48.

Pieraccini, M., Miccinesi, L., 2019. Ground-based radar interferometry: A bibliographic review. Remote Sens. 11, 1029.

Rodrigues, D.V.Q., Li, C., 2021. A Review on Low-Cost Microwave Doppler Radar Systems for Structural Health Monitoring. Sensors 2021, Vol. 21, Page 2612 21, 2612. doi.org/10.3390/S21082612

Rudolf, H., Leva, D., Tarchi, D., Sieber, A.J., 1999. Mobile and versatile SAR system, in: International Geoscience and Remote Sensing Symposium (IGARSS). IEEE, pp. 592–594. doi.org/10.1109/igarss.1999.773575

Tarchi, D., Oliveri, F., Sammartino, P.F., 2012. MIMO radar and ground-based SAR imaging systems: Equivalent approaches for remote sensing. IEEE Trans. Geosci. Remote Sens. 51, 425–435.

Tarchi, D., Rudolf, H., Luzi, G., Chiarantini, L., Coppo, P., Sieber, A.J., 1999. SAR interferometry for structural changes detection: a demonstration test on a dam, in: International Geoscience and Remote Sensing Symposium (IGARSS). IEEE, pp. 1522–1524. doi.org/10.1109/igarss.1999.772006

Wang, Y., Hong, W., Zhang, Y., Lin, Y., Li, Y., Bai, Z., Zhang, Q., Lv, S., Liu, H., Song, Y., 2020. Ground-Based Differential Interferometry SAR: A Review. IEEE Geosci. Remote Sens. Mag. 8, 43–70.

Yanik, M.E., Wang, D., Torlak, M., 2020. Development and Demonstration of MIMO-SAR mmWave Imaging Testbeds. IEEE Access 8, 126019–126038. doi.org/10.1109/ACCESS.2020.3007877